

# The Single-Cloud Star Formation Relation

Riwaj Pokhrel (✉ [riwajpokhrel@gmail.com](mailto:riwajpokhrel@gmail.com))

University of Toledo <https://orcid.org/0000-0002-0557-7349>

---

## Physical Sciences - Article

**Keywords:** Kennicutt-Schmidt Relation, Formation Rates, Gas Densities, Molecular Clouds, Turbulence, Protostellar Outflows

**Posted Date:** November 23rd, 2020

**DOI:** <https://doi.org/10.21203/rs.3.rs-108727/v1>

**License:** © ⓘ This work is licensed under a Creative Commons Attribution 4.0 International License.

[Read Full License](#)

---

**Version of Record:** A version of this preprint was published at The Astrophysical Journal Letters on May 1st, 2021. See the published version at <https://doi.org/10.3847/2041-8213/abf564>.

# The Single-Cloud Star Formation Relation

Riwaj Pokhrel<sup>1,\*</sup>, Robert A. Gutermuth<sup>2</sup>, Mark R. Krumholz<sup>3,4</sup>, Christoph Federrath<sup>3,4</sup>, Mark Heyer<sup>2</sup>, Shivan Khullar<sup>5,6</sup>, S. Thomas Megeath<sup>1</sup>, Philip C. Myers<sup>7</sup>, Stella S. R. Offner<sup>8</sup>, Judith L. Pipher<sup>9</sup>, William J. Fischer<sup>10</sup>, Thomas Henning<sup>11</sup>, and Joseph L. Hora<sup>7</sup>

<sup>1</sup>Ritter Astrophysical Research Center, Department of Physics and Astronomy, University of Toledo, Toledo, OH 43606, USA

<sup>2</sup>Department of Astronomy, University of Massachusetts, 710 North Pleasant Street, Amherst, MA 01003, USA

<sup>3</sup>Research School of Astronomy and Astrophysics, Australian National University, Cotter Rd., Weston Creek ACT 2611, Australia

<sup>4</sup>ARC Centre of Excellence for Astronomy in 3 Dimensions (ASTRO-3D), Canberra ACT 2601, Australia

<sup>5</sup>Canadian Institute for Theoretical Astrophysics, 60 St. George Street, University of Toronto, Toronto ON M5S 3H4, Canada

<sup>6</sup>David A. Dunlap Department of Astronomy and Astrophysics, University of Toronto, 50 St George Street, Toronto, Ontario, M5S 3H4, Canada

<sup>7</sup>Center for Astrophysics, Harvard & Smithsonian, 60 Garden Street, Cambridge, MA 02138, USA

<sup>8</sup>Department of Astronomy, The University of Texas at Austin, 2500 Speedway, Austin, TX 78712, USA

<sup>9</sup>Department of Physics and Astronomy, University of Rochester, Rochester, NY 14627, USA

<sup>10</sup>Space Telescope Science Institute, Baltimore, MD 21218, USA

<sup>11</sup>Max-Planck-Institute for Astronomy, Königstuhl 17, D-69117 Heidelberg, Germany

\*e-mail: Riwaj.Pokhrel@UToledo.Edu, riwajpokhrel@gmail.com

## ABSTRACT

One of the most important and well-established empirical results in astronomy is the so-called Kennicutt-Schmidt (KS) relation between the density of interstellar gas and the rate at which that gas forms stars<sup>1–4</sup>. While a tight correlation between these quantities has long been measured at galactic scales, the difficulty of measuring star formation rates and gas densities over a large dynamic range at sub-galactic scales has thus far precluded a definitive determination of whether the same relationship holds within individual star-forming clouds. In this article we use a new, high-accuracy catalogue of young stellar objects from *Spitzer* combined with new, high-dynamic range maps of twelve nearby ( $<1.5$  kpc) molecular clouds from *Herschel*<sup>5</sup> to re-examine the KS relation within individual molecular clouds. We find a tight, linear correlation between clouds' star formation rate per unit area and their gas surface density normalised by the gas free-fall time. The measured relation extends over more than two orders of magnitude within each cloud, and is nearly identical in each of the twelve clouds, implying a constant star formation efficiency per free-fall time  $\epsilon_{\text{ff}} \approx 0.026$ . The finding of a universal correlation within individual molecular clouds, including clouds that contain no massive stars or massive stellar feedback, favours models in which star formation is regulated by local processes such as turbulence or protostellar outflows<sup>6–8</sup>, and disfavors models in which star formation is regulated primarily by galaxy properties or supernova feedback on galactic scales<sup>9–11</sup>.

## 1 Introduction

In galactic discs, there is a well-established correlation between the gas mass and star formation rate per unit area, when both quantities are measured in kpc-scale or larger patches<sup>2–4</sup>; this correlation is known as the KS relation. However, the correlation worsens as one measures progressively smaller regions, and there is little correlation between the carbon monoxide and ionising or far-infrared luminosities – standard proxies for gas mass and star formation rate, respectively – of individual molecular clouds or filaments  $\lesssim 100$  pc in size<sup>12–15</sup>. It remains uncertain whether this decorrelation is the result of a true spread in the star formation rate per unit mass among clouds<sup>16</sup>, or if it is due to the failure of our proxies for mass and star formation rate. The latter is possible because we most often estimate star formation rate using the luminosity of massive stars, and this proxy underestimates the true star formation rate until the stellar population is old enough ( $\sim 5$ -10 Myr) to have reached statistical steady state between the formation of new massive stars and the deaths of older ones. Conversely, massive stars can rapidly disperse the gas from which they formed, and if we observe a stellar population where dispersal is well underway, we will underestimate the mass of gas that was present when the stars formed. Thus analyses based on massive stars will tend to underestimate the star formation rate per unit mass in young clouds and overestimate it in old clouds. When we measure the KS

relation in kpc-scale patches, we average over large numbers of clouds at random ages, these errors cancel, and we recover the correct mean star formation rate per unit mass. However, the errors for individual clouds might nonetheless be substantial, artificially creating scatter in the KS relation at smaller scales<sup>13,17</sup>.

Whether the observed large scatter in the KS relation at small scales indicates a real scatter in star formation rate per unit mass, or whether it is simply an artefact of the observational errors described above, has profound implications for our understanding of the mechanisms by which star formation is regulated. If it is real, this suggests that the KS relation on galactic scales is due to feedback processes acting at similar scales, most likely the balance between gravity and supernovae<sup>9–11</sup> (SNe), and individual clouds are free to collapse to stars with high efficiency; indeed, the lack of a KS relation within individual clouds is a direct prediction of such models<sup>16</sup>. On the other hand, if a KS relation does hold within single clouds, particularly those containing no stars massive enough to produce SNe, this implies that some smaller-scale or more universal mechanism inhibits star formation within individual molecular clouds, for example turbulence, magnetic fields, or protostellar outflows<sup>6,7</sup>.

A natural experiment for deciding between these possibilities is to search for a KS relation within individual molecular clouds using counts of the recently formed stars or protostars (identified by bright infrared emission from circumstellar dust) rather than the luminosities of massive stars as a proxy for star formation rate, thereby avoiding the problems of finite luminosity buildup time and rapid cloud dispersal. Such studies generally do find a reasonable correlation between the number of young stellar objects (YSOs) in a cloud and its mass, or its mass divided by its mean-density free-fall time<sup>8,18–21</sup>. However, these are correlations across many distinct clouds, not within a single cloud, which is the true test of the KS relation. Searches for a single-cloud KS relation have thus far met with mixed results<sup>18,19,22,23</sup>, as they have all been hampered by their reliance on YSO catalogues with complex and poorly-understood sensitivity limits, and on extinction maps to measure mass within clouds. Such maps span a relatively limited dynamic range in column density. The most complete study to date is that of ref.<sup>5</sup>, which uses the same underlying data that we will use here, and which does find a strong correlation between gas and YSO surface densities. However, their analysis technique examines the density of gas around stars on a star-by-star basis, and thus cannot easily determine whether the KS relation is the same from cloud to cloud, or whether there is dependence on additional parameters such as the cloud free-fall time. Thus while this result is suggestive, it does not settle the question of whether a cloud-scale KS relation exists, or what form it might take.

## 2 Results

In this article we re-examine the KS relation within single clouds using a uniformly reduced catalog of the protostars from the *Spitzer* Extended Solar Neighborhood Archive (SESNA) and uniformly reduced gas column density maps based on dust emission from *Herschel* for 12 molecular clouds that cover very different star formation environments<sup>5</sup>. Compared to previous samples, our YSO catalogue and dust maps probe a much larger dynamic range in gas column density and star formation rate and have well-modelled sensitivity and completeness, allowing a much more sensitive test of the single-cloud KS relation. Full details of the protostellar catalogue and maps are provided in the Methods section, and we provide a detailed comparison between our data and those used in earlier searches for a single-cloud KS relation in the Supplementary Information.

We show our data for one example cloud, Mon R2 GMC, in Figure 1. On the observed map, we define a series of contours at different gas column densities  $N(\text{H}_2)$ , at levels chosen using the procedure described in Methods. Within each contour, we measure the enclosed area  $A$ , the enclosed gas mass  $M_{\text{gas}}$ , and the number of enclosed protostars  $N_{\text{PS}}$  (Figure 1c). We adopt  $M_{\text{PS}} \approx 0.5 M_{\odot}$  for the mean mass of protostars in our catalogue<sup>24</sup>, and the duration of the protostellar phase during which newborn stars will be included in our catalogue is  $t_{\text{PS}} \approx 0.5 \text{ Myr}$ <sup>25</sup>; see Methods for details. Consequently, we can compute the star formation rate within each contour as  $\text{SFR} = N_{\text{PS}} M_{\text{PS}} / t_{\text{PS}}$ .

In Figure 2a we plot the relationship between the star formation rate surface density  $\Sigma_{\text{SFR}} = \text{SFR} / A$  and gas surface density  $\Sigma_{\text{gas}} = M_{\text{gas}} / A$  defined by our contours. Clearly the relation is approximately linear in log-log, and we report the results of a least-squares fit of the data to a linear functional form in Table 1. We fit only the data that comes from column density contours  $< 3 \times 10^{22} \text{ cm}^{-2}$ , since above this limit the contours and number of protostars enclosed become very small, and Poisson errors in  $\Sigma_{\text{SFR}}$  become large. Considering all 12 clouds, the median best-fit slope is 2.08, and near the centre of the observed data range (gas surface density  $\Sigma_{\text{gas}} = 10^{2.5} M_{\odot} \text{ pc}^{-2}$ ), the interquartile range (IQR) of the measured values of  $\log \Sigma_{\text{SFR}}$  across all clouds is 0.36. We show the line corresponding to our median fit parameters, with this scatter, in Figure 2a.

While the surface densities of gas and star formation are the quantities most directly accessible from observations, most theoretical models that predict the existence of a KS relation for single clouds predict a dependence on the gas free-fall time<sup>6,21,26,27</sup>, which depends on the volume density; incorporating the free-fall time also gives a tighter correlation when measuring the cloud-to-cloud KS relation<sup>8,20</sup>. In order to estimate the free-fall time, we follow ref.<sup>8</sup> in computing the density of the material within each surface density contour by assuming that the unseen dimension along the line of sight is comparable to the two dimensions observed in the plane of the sky, so that  $\rho = 3\sqrt{\pi} M_{\text{gas}} / 4A^{3/2}$ ; we then compute the free-fall time as  $t_{\text{ff}} = \sqrt{3\pi / 32G\rho}$ . This amounts to assuming that the region being studied is a sphere in three dimensions, and recent works by Z. Hu et al. (in prep.) shows that this assumption is likely responsible for adding a scatter of  $\sim 0.2$  to estimates

of  $\log \epsilon_{\text{ff}}$ . Figure 2b shows the relationship between  $\Sigma_{\text{SFR}}$  and  $\Sigma_{\text{gas}}/t_{\text{ff}}$ , and Table 1 shows the results of fitting a linear (in logarithm) relationship between these quantities. It is immediately clear that the scatter is much smaller for this relationship than for the one between  $\Sigma_{\text{SFR}}$  and  $\Sigma_{\text{gas}}$  alone; quantitatively, the IQR of the data is reduced from 0.36 to 0.14 (computed at  $\Sigma_{\text{gas}}/t_{\text{ff}} = 10^{2.5} M_{\odot} \text{pc}^{-2} \text{Myr}^{-1}$ ) by inclusion of the free-fall time. Moreover, the relationship is now linear, with a median best-fit slope of 0.99. This finding, coupled with the theoretical predictions for a linear relationship, motivates us to carry out a fit where we fix the slope to unity and fit only the offset, so the functional form is

$$\log \Sigma_{\text{SFR}} = \log (\Sigma_{\text{gas}}/t_{\text{ff}}) + \log \epsilon_{\text{ff}}, \quad (1)$$

where  $\epsilon_{\text{ff}}$  is the fraction of the gas mass converted to stars per free-fall time. The resulting fits are indistinguishable within the error bars from those where we allow the slope to vary (see Table 1). We show the fit using the median value of  $\epsilon_{\text{ff}} \approx 0.026$  in Figure 2b.

We further examine the value of  $\epsilon_{\text{ff}}$  as a function of column density for each of our clouds in Figure 3. We construct this Figure following the method of ref.<sup>28</sup>, whereby we vary the contour level as shown in Figure 1, and within each contour we measure  $\epsilon_{\text{ff}} = \text{SFR}/(M_{\text{gas}}/t_{\text{ff}})$ , where the values of SFR,  $M_{\text{gas}}$ , and  $t_{\text{ff}}$  are the values within the contour. The Figure shows how  $\epsilon_{\text{ff}}$  varies with mean gas column density within the corresponding contour  $\Sigma_{\text{gas}}$ . We find no evidence for any threshold at which star formation becomes efficient, i.e., where  $\epsilon_{\text{ff}}$  rises substantially. This is contrary to some earlier analyses using much more limited data<sup>29–31</sup>. Instead we find that in almost all clouds  $\epsilon_{\text{ff}}$  is nearly constant over  $\approx 1$  decade in column density from  $\approx 100$ – $1000 M_{\odot} \text{pc}^{-2}$ , and that at column densities  $\gtrsim 1000 M_{\odot} \text{pc}^{-2}$  the value of  $\epsilon_{\text{ff}}$  decreases rather than increases.

The decrease in  $\epsilon_{\text{ff}}$  at high column density is contrary to the naive expectation that star formation should become more rather than less efficient in denser gas. However, it seems likely that the drop in apparent  $\epsilon_{\text{ff}}$  is not indicative of a true decline in star formation efficiency but is rather a result of one of three possible effects. First, the surface densities above which  $\epsilon_{\text{ff}}$  decreases tend to correspond to contours with rather small areas, such that the projected size on the plane of the sky is  $\sim 1$  pc (Figure 1). The YSOs we use to estimate the star formation rate have a lifetime of  $t_{\text{PS}} \approx 0.5$  Myr, and over this time scale an object moving at a speed of  $\approx 2 \text{ km s}^{-1}$ , well within the typical velocity dispersion of YSOs<sup>32</sup>, will move  $\approx 1$  pc. Thus we might underestimate star formation rates in the smallest contours because YSOs have moved out of them. A second possible explanation is that protostellar lifetimes might not be independent of density as we have assumed. Protostellar luminosities are observed to be higher in dense regions of molecular clouds<sup>33,34</sup>, and it is possible that this is a signature of more rapid accretion that could in turn lead to more rapid progression through the evolutionary phase selected by our catalogue. In this case our method would lead us to somewhat underestimate  $\epsilon_{\text{ff}}$  in the densest regions we survey. A third possible explanation is that the densest parts of star-forming regions are also sites of bright and complex emission in the infrared that can contribute to locally reduced YSO sensitivity<sup>35</sup>. Our SENSEA catalogue is more sensitive than previous ones in these regions, as we show in the Supplementary Information, but we may still suffer from some incompleteness in the densest regions. Again, this would cause us to underestimate  $\epsilon_{\text{ff}}$ .

### 3 Implications

Our results demonstrate that star formation within individual molecular clouds follows a tight KS relation, characterised by a linear relationship between star formation rate and mass normalised by free-fall time. The proportionality constant between these quantities has a median value  $\epsilon_{\text{ff}} \approx 0.026$ , and the scatter is only  $\approx 0.14$  in the logarithm of the star formation rate. This relationship is essentially the same in all the molecular clouds we studied. This is significant because the clouds themselves span a huge range of properties: for example, the Perseus and Ophiuchus clouds contain no stars with significant ionising luminosities or winds, while Cep OB3 and Orion-A and -B are sites of ongoing massive star formation.

The small scatter in  $\epsilon_{\text{ff}}$  we have measured rules out models in which star formation is regulated only at galactic scales, and not within individual clouds. For example, ref.<sup>36</sup> propose that molecular clouds are collapsing and that, as a result, the star formation rate within them increases with time as  $\text{SFR} \propto t^2$ ; ref.<sup>16</sup> shows that the observed dispersion in  $\log \epsilon_{\text{ff}}$  predicted by this model is 0.54, a factor of  $\approx 3$  larger than we observe. By contrast, a model in which there is no collapse and thus  $\epsilon_{\text{ff}}$  does not increase yields a dispersion in  $\log \epsilon_{\text{ff}}$  of 0.16, very close to what we observe. Thus our observations strongly favour the existence of a mechanism that keeps  $\epsilon_{\text{ff}}$  close to constant across all local molecular clouds. Moreover, this mechanism must not depend on the feedback provided by massive stars, since many of the clouds we have observed contain no massive stars.

## References

1. Schmidt, M. The Rate of Star Formation. *Astrophys. J.* **129**, 243, DOI: [10.1086/146614](https://doi.org/10.1086/146614) (1959).
2. Kennicutt, J., Robert C. The Global Schmidt Law in Star-forming Galaxies. *Astrophys. J.* **498**, 541–552, DOI: [10.1086/305588](https://doi.org/10.1086/305588) (1998). [astro-ph/9712213](https://arxiv.org/abs/astro-ph/9712213).
3. Bigiel, F. *et al.* The Star Formation Law in Nearby Galaxies on Sub-Kpc Scales. *Astron. J.* **136**, 2846–2871, DOI: [10.1088/0004-6256/136/6/2846](https://doi.org/10.1088/0004-6256/136/6/2846) (2008). [0810.2541](https://arxiv.org/abs/0810.2541).
4. Leroy, A. K. *et al.* Molecular Gas and Star Formation in nearby Disk Galaxies. *Astron. J.* **146**, 19, DOI: [10.1088/0004-6256/146/2/19](https://doi.org/10.1088/0004-6256/146/2/19) (2013). [1301.2328](https://arxiv.org/abs/1301.2328).
5. Pokhrel, R. *et al.* Star-Gas Surface Density Correlations in 12 Nearby Molecular Clouds. I. Data Collection and Star-sampled Analysis. *Astrophys. J.* **896**, 60, DOI: [10.3847/1538-4357/ab92a2](https://doi.org/10.3847/1538-4357/ab92a2) (2020). [2005.05466](https://arxiv.org/abs/2005.05466).
6. Krumholz, M. R. & McKee, C. F. A General Theory of Turbulence-regulated Star Formation, from Spirals to Ultraluminous Infrared Galaxies. *Astrophys. J.* **630**, 250–268, DOI: [10.1086/431734](https://doi.org/10.1086/431734) (2005). [astro-ph/0505177](https://arxiv.org/abs/astro-ph/0505177).
7. Federrath, C. & Klessen, R. S. The Star Formation Rate of Turbulent Magnetized Clouds: Comparing Theory, Simulations, and Observations. *Astrophys. J.* **761**, 156, DOI: [10.1088/0004-637X/761/2/156](https://doi.org/10.1088/0004-637X/761/2/156) (2012). [1209.2856](https://arxiv.org/abs/1209.2856).
8. Krumholz, M. R., Dekel, A. & McKee, C. F. A Universal, Local Star Formation Law in Galactic Clouds, nearby Galaxies, High-redshift Disks, and Starbursts. *Astrophys. J.* **745**, 69, DOI: [10.1088/0004-637X/745/1/69](https://doi.org/10.1088/0004-637X/745/1/69) (2012). [1109.4150](https://arxiv.org/abs/1109.4150).
9. Hopkins, P. F., Quataert, E. & Murray, N. Self-regulated star formation in galaxies via momentum input from massive stars. *Mon. Not. R. Astron. Soc.* **417**, 950–973, DOI: [10.1111/j.1365-2966.2011.19306.x](https://doi.org/10.1111/j.1365-2966.2011.19306.x) (2011). [1101.4940](https://arxiv.org/abs/1101.4940).
10. Ostriker, E. C. & Shetty, R. Maximally Star-forming Galactic Disks. I. Starburst Regulation Via Feedback-driven Turbulence. *Astrophys. J.* **731**, 41–+, DOI: [10.1088/0004-637X/731/1/41](https://doi.org/10.1088/0004-637X/731/1/41) (2011). [1102.1446](https://arxiv.org/abs/1102.1446).
11. Faucher-Giguère, C.-A., Quataert, E. & Hopkins, P. F. Feedback-regulated star formation in molecular clouds and galactic discs. *Mon. Not. R. Astron. Soc.* **433**, 1970–1990, DOI: [10.1093/mnras/stt866](https://doi.org/10.1093/mnras/stt866) (2013). [1301.3905](https://arxiv.org/abs/1301.3905).
12. Mooney, T. J. & Solomon, P. M. Star formation rates and the far-infrared luminosity of Galactic molecular clouds. *Astrophys. J. L.* **334**, L51–L54, DOI: [10.1086/185310](https://doi.org/10.1086/185310) (1988).
13. Kruijssen, J. M. D. & Longmore, S. N. An uncertainty principle for star formation - I. Why galactic star formation relations break down below a certain spatial scale. *Mon. Not. R. Astron. Soc.* **439**, 3239–3252, DOI: [10.1093/mnras/stu098](https://doi.org/10.1093/mnras/stu098) (2014). [1401.4459](https://arxiv.org/abs/1401.4459).
14. Ochsendorf, B. B., Meixner, M., Roman-Duval, J., Rahman, M. & Evans, N. J., II. What Sets the Massive Star Formation Rates and Efficiencies of Giant Molecular Clouds? *Astrophys. J.* **841**, 109, DOI: [10.3847/1538-4357/aa704a](https://doi.org/10.3847/1538-4357/aa704a) (2017). [1704.06965](https://arxiv.org/abs/1704.06965).
15. Zhang, M., Kainulainen, J., Mattern, M., Fang, M. & Henning, T. Star-forming content of the giant molecular filaments in the Milky Way. *Astron. Astrophys.* **622**, A52, DOI: [10.1051/0004-6361/201732400](https://doi.org/10.1051/0004-6361/201732400) (2019). [1811.02197](https://arxiv.org/abs/1811.02197).
16. Lee, E. J., Miville-Deschênes, M.-A. & Murray, N. W. Observational Evidence of Dynamic Star Formation Rate in Milky Way Giant Molecular Clouds. *Astrophys. J.* **833**, 229, DOI: [10.3847/1538-4357/833/2/229](https://doi.org/10.3847/1538-4357/833/2/229) (2016). [1608.05415](https://arxiv.org/abs/1608.05415).
17. Feldmann, R. & Gnedin, N. Y. On the Time Variability of the Star Formation Efficiency. *Astrophys. J. L.* **727**, L12+, DOI: [10.1088/2041-8205/727/1/L12](https://doi.org/10.1088/2041-8205/727/1/L12) (2011). [1009.5674](https://arxiv.org/abs/1009.5674).
18. Lada, C. J., Forbrich, J., Lombardi, M. & Alves, J. F. Star Formation Rates in Molecular Clouds and the Nature of the Extragalactic Scaling Relations. *Astrophys. J.* **745**, 190, DOI: [10.1088/0004-637X/745/2/190](https://doi.org/10.1088/0004-637X/745/2/190) (2012). [1112.4466](https://arxiv.org/abs/1112.4466).
19. Evans, I., Neal J., Heiderman, A. & Vutisalchavakul, N. Star Formation Relations in Nearby Molecular Clouds. *Astrophys. J.* **782**, 114, DOI: [10.1088/0004-637X/782/2/114](https://doi.org/10.1088/0004-637X/782/2/114) (2014). [1401.3287](https://arxiv.org/abs/1401.3287).
20. Heyer, M. *et al.* The rate and latency of star formation in dense, massive clumps in the Milky Way. *Astron. Astrophys.* **588**, A29, DOI: [10.1051/0004-6361/201527681](https://doi.org/10.1051/0004-6361/201527681) (2016). [1601.06875](https://arxiv.org/abs/1601.06875).
21. Krumholz, M. R., McKee, C. F. & Bland-Hawthorn, J. Star Clusters Across Cosmic Time. *ARA@AND@A* **57**, 227–303, DOI: [10.1146/annurev-astro-091918-104430](https://doi.org/10.1146/annurev-astro-091918-104430) (2019). [1812.01615](https://arxiv.org/abs/1812.01615).
22. Gutermuth, R. A. *et al.* A Correlation between Surface Densities of Young Stellar Objects and Gas in Eight Nearby Molecular Clouds. *Astrophys. J.* **739**, 84, DOI: [10.1088/0004-637X/739/2/84](https://doi.org/10.1088/0004-637X/739/2/84) (2011). [1107.0966](https://arxiv.org/abs/1107.0966).
23. Willis, S. *et al.* The Schmidt Law in Six Galactic Massive Star-forming Regions. *Astrophys. J.* **809**, 87, DOI: [10.1088/0004-637X/809/1/87](https://doi.org/10.1088/0004-637X/809/1/87) (2015).



24. Evans, N. J., II *et al.* The Spitzer c2d Legacy Results: Star-Formation Rates and Efficiencies; Evolution and Lifetimes. *Astrophys. J. Supp.* **181**, 321–350, DOI: [10.1088/0067-0049/181/2/321](https://doi.org/10.1088/0067-0049/181/2/321) (2009). [0811.1059](https://arxiv.org/abs/0811.1059).
25. Dunham, M. M. *et al.* Young Stellar Objects in the Gould Belt. *Astrophys. J. Supp.* **220**, 11, DOI: [10.1088/0067-0049/220/1/11](https://doi.org/10.1088/0067-0049/220/1/11) (2015). [1508.03199](https://arxiv.org/abs/1508.03199).
26. Padoan, P., Haugbølle, T. & Nordlund, Å. A Simple Law of Star Formation. *Astrophys. J. L.* **759**, L27, DOI: [10.1088/2041-8205/759/2/L27](https://doi.org/10.1088/2041-8205/759/2/L27) (2012). [1208.3758](https://arxiv.org/abs/1208.3758).
27. Federrath, C. On the universality of supersonic turbulence. *Mon. Not. R. Astron. Soc.* **436**, 1245–1257, DOI: [10.1093/mnras/stt1644](https://doi.org/10.1093/mnras/stt1644) (2013). [1306.3989](https://arxiv.org/abs/1306.3989).
28. Khullar, S., Krumholz, M. R., Federrath, C. & Cunningham, A. J. Determining star formation thresholds from observations. *Mon. Not. R. Astron. Soc.* **488**, 1407–1415, DOI: [10.1093/mnras/stz1800](https://doi.org/10.1093/mnras/stz1800) (2019). [1902.00934](https://arxiv.org/abs/1902.00934).
29. Lada, C. J., Lombardi, M. & Alves, J. F. On the Star Formation Rates in Molecular Clouds. *Astrophys. J.* **724**, 687–693, DOI: [10.1088/0004-637X/724/1/687](https://doi.org/10.1088/0004-637X/724/1/687) (2010). [1009.2985](https://arxiv.org/abs/1009.2985).
30. Heiderman, A., Evans, I., Neal J., Allen, L. E., Huard, T. & Heyer, M. The Star Formation Rate and Gas Surface Density Relation in the Milky Way: Implications for Extragalactic Studies. *Astrophys. J.* **723**, 1019–1037, DOI: [10.1088/0004-637X/723/2/1019](https://doi.org/10.1088/0004-637X/723/2/1019) (2010). [1009.1621](https://arxiv.org/abs/1009.1621).
31. Könyves, V. *et al.* A census of dense cores in the Aquila cloud complex: SPIRE/PACS observations from the Herschel Gould Belt survey. *Astron. Astrophys.* **584**, A91, DOI: [10.1051/0004-6361/201525861](https://doi.org/10.1051/0004-6361/201525861) (2015). [1507.05926](https://arxiv.org/abs/1507.05926).
32. Covey, K. R., Greene, T. P., Doppmann, G. W. & Lada, C. J. The Radial Velocity Distribution of Class I and Flat-Spectrum Protostars. *Astron. J.* **131**, 512–519, DOI: [10.1086/498064](https://doi.org/10.1086/498064) (2006). [astro-ph/0509264](https://arxiv.org/abs/astro-ph/0509264).
33. Kryukova, E. *et al.* The Dependence of Protostellar Luminosity on Environment in the Cygnus-X Star-forming Complex. *Astron. J.* **148**, 11, DOI: [10.1088/0004-6256/148/1/11](https://doi.org/10.1088/0004-6256/148/1/11) (2014). [1405.0004](https://arxiv.org/abs/1405.0004).
34. Kirk, H. *et al.* The JCMT Gould Belt Survey: Dense Core Clusters in Orion B. *Astrophys. J.* **821**, 98, DOI: [10.3847/0004-637X/821/2/98](https://doi.org/10.3847/0004-637X/821/2/98) (2016). [1602.00707](https://arxiv.org/abs/1602.00707).
35. Megeath, S. T. *et al.* The Spitzer Space Telescope Survey of the Orion A and B Molecular Clouds. II. The Spatial Distribution and Demographics of Dusty Young Stellar Objects. *Astron. J.* **151**, 5, DOI: [10.3847/0004-6256/151/1/5](https://doi.org/10.3847/0004-6256/151/1/5) (2016). [1511.01202](https://arxiv.org/abs/1511.01202).
36. Murray, N. & Chang, P. Star Formation in Self-gravitating Turbulent Fluids. *Astrophys. J.* **804**, 44, DOI: [10.1088/0004-637X/804/1/44](https://doi.org/10.1088/0004-637X/804/1/44) (2015). [1407.6373](https://arxiv.org/abs/1407.6373).
37. Pokhrel, R. *et al.* A Herschel-SPIRE survey of the Mon R2 giant molecular cloud: analysis of the gas column density probability density function. *Mon. Not. R. Astron. Soc.* **461**, 22–35, DOI: [10.1093/mnras/stw1303](https://doi.org/10.1093/mnras/stw1303) (2016). [1606.01752](https://arxiv.org/abs/1606.01752).
38. Fazio, G. G. *et al.* The Infrared Array Camera (IRAC) for the Spitzer Space Telescope. *Astrophys. J. Supp.* **154**, 10–17, DOI: [10.1086/422843](https://doi.org/10.1086/422843) (2004). [astro-ph/0405616](https://arxiv.org/abs/astro-ph/0405616).
39. Rieke, G. H. *et al.* The Multiband Imaging Photometer for Spitzer (MIPS). *Astrophys. J. Supp.* **154**, 25–29, DOI: [10.1086/422717](https://doi.org/10.1086/422717) (2004).
40. Skrutskie, M. F. *et al.* The Two Micron All Sky Survey (2MASS). *Astron. J.* **131**, 1163–1183, DOI: [10.1086/498708](https://doi.org/10.1086/498708) (2006).
41. Lucas, P. W. *et al.* The UKIDSS Galactic Plane Survey. *Mon. Not. R. Astron. Soc.* **391**, 136–163, DOI: [10.1111/j.1365-2966.2008.13924.x](https://doi.org/10.1111/j.1365-2966.2008.13924.x) (2008). [0712.0100](https://arxiv.org/abs/0712.0100).
42. Gutermuth, R. A. *et al.* A Spitzer Survey of Young Stellar Clusters Within One Kiloparsec of the Sun: Cluster Core Extraction and Basic Structural Analysis. *Astrophys. J. Supp.* **184**, 18–83, DOI: [10.1088/0067-0049/184/1/18](https://doi.org/10.1088/0067-0049/184/1/18) (2009). [0906.0201](https://arxiv.org/abs/0906.0201).
43. Gutermuth, R. A. & Heyer, M. A 24  $\mu$ m Point Source Catalog of the Galactic Plane from Spitzer/MIPSGAL. *Astron. J.* **149**, 64, DOI: [10.1088/0004-6256/149/2/64](https://doi.org/10.1088/0004-6256/149/2/64) (2015). [1412.4751](https://arxiv.org/abs/1412.4751).
44. Megeath, S. T. *et al.* The Spitzer Space Telescope Survey of the Orion A and B Molecular Clouds. I. A Census of Dusty Young Stellar Objects and a Study of Their Mid-infrared Variability. *Astron. J.* **144**, 192, DOI: [10.1088/0004-6256/144/6/192](https://doi.org/10.1088/0004-6256/144/6/192) (2012). [1209.3826](https://arxiv.org/abs/1209.3826).
45. Gutermuth, R. A. *et al.* Spitzer Observations of NGC 1333: A Study of Structure and Evolution in a Nearby Embedded Cluster. *Astrophys. J.* **674**, 336–356, DOI: [10.1086/524722](https://doi.org/10.1086/524722) (2008). [0710.1860](https://arxiv.org/abs/0710.1860).

46. Ossenkopf, V. & Henning, T. Dust opacities for protostellar cores. *Astron. Astrophys.* **291**, 943–959 (1994).
47. Nieva, M.-F. & Przybilla, N. Present-day cosmic abundances. A comprehensive study of nearby early B-type stars and implications for stellar and Galactic evolution and interstellar dust models. *Astron. Astrophys.* **539**, A143, DOI: [10.1051/0004-6361/201118158](https://doi.org/10.1051/0004-6361/201118158) (2012). 1203.5787.

Cloud	A <sub>V</sub> level (mag)		log Σ <sub>SFR</sub> = a log Σ <sub>gas</sub> + b		log Σ <sub>SFR</sub> = a log (Σ <sub>gas</sub> /t <sub>ff</sub> ) + b		log Σ <sub>SFR</sub> = log (Σ <sub>gas</sub> /t <sub>ff</sub> ) + log ε <sub>ff</sub>
	Min	Max	a	b	a	b	
Ophiuchus	3.0	55.5	1.83±0.03	-3.24±0.08	0.87±0.02	-1.11±0.05	-1.44±0.12
Perseus	2.0	92.0	1.88±0.02	-3.54±0.05	0.92±0.01	-1.31±0.03	-1.51±0.13
Orion-A	3.0	99.5	2.14±0.01	-5.13±0.03	1.04±0.01	-2.20±0.01	-2.00±0.04
Orion-B	3.0	90.5	2.14±0.01	-4.58±0.04	1.01±0.01	-1.84±0.02	-1.77±0.13
Aquila-North	4.0	99.5	2.08±0.03	-4.23±0.07	1.01±0.01	-1.71±0.04	-1.60±0.07
Aquila-South	3.0	99.5	2.20±0.01	-4.62±0.02	1.03±0.01	-1.75±0.02	-1.55±0.03
NGC 2264	3.0	99.5	1.71±0.02	-3.64±0.05	0.86±0.01	-1.55±0.03	-1.85±0.09
S140	2.0	53.0	2.09±0.02	-4.17±0.06	0.97±0.01	-1.61±0.03	-1.57±0.06
AFGL 490	4.0	40.0	1.44±0.06	-2.55±0.15	0.67±0.03	-0.82±0.08	-1.70±0.21
Cep OB3	3.0	57.0	2.36±0.02	-4.93±0.05	1.03±0.01	-1.73±0.03	-1.52±0.04
Mon R2	2.0	94.0	1.71±0.04	-3.41±0.09	0.82±0.02	-1.25±0.05	-1.80±0.24
Cygnus-X	3.0	99.5	2.38±0.02	-5.25±0.06	1.06±0.01	-1.49±0.02	-1.37±0.19
Median			2.08	-4.2	0.99	-1.58	-1.59
Mean			2.0	-4.11	0.94	-1.53	-1.64
IQR			0.36		0.14		

**Table 1.** Best-fit parameters with errors. The column A<sub>V</sub> indicates the range in visual extinction over which the relationship is measured. In each remaining group of columns, the equation at the top indicates the functional form being fit, and the columns under it give the best-fit parameters for each cloud; numerical values given are for Σ<sub>gas</sub> in units of M<sub>⊙</sub> pc<sup>-2</sup>, t<sub>ff</sub> in units of Myr, and Σ<sub>SFR</sub> in units of M<sub>⊙</sub> pc<sup>-2</sup> Myr<sup>-1</sup>. The entries at the bottom of the table give the median and mean of the fit values, and the interquartile range (IQR), i.e., between the 25th and 75th percentile of the data, evaluated near the centre of the observed data range, at Σ<sub>gas</sub> = 10<sup>2.5</sup> M<sub>⊙</sub> pc<sup>-2</sup> and t<sub>ff</sub> = 1 Myr. Note that the IQR of the data is the same for the two right-hand columns, since these two functional forms use the same data values on the horizontal and vertical axes. The entries for ε<sub>ff</sub> correspond to the mean and standard deviation of ε<sub>ff</sub> for each cloud (see Figure 3).



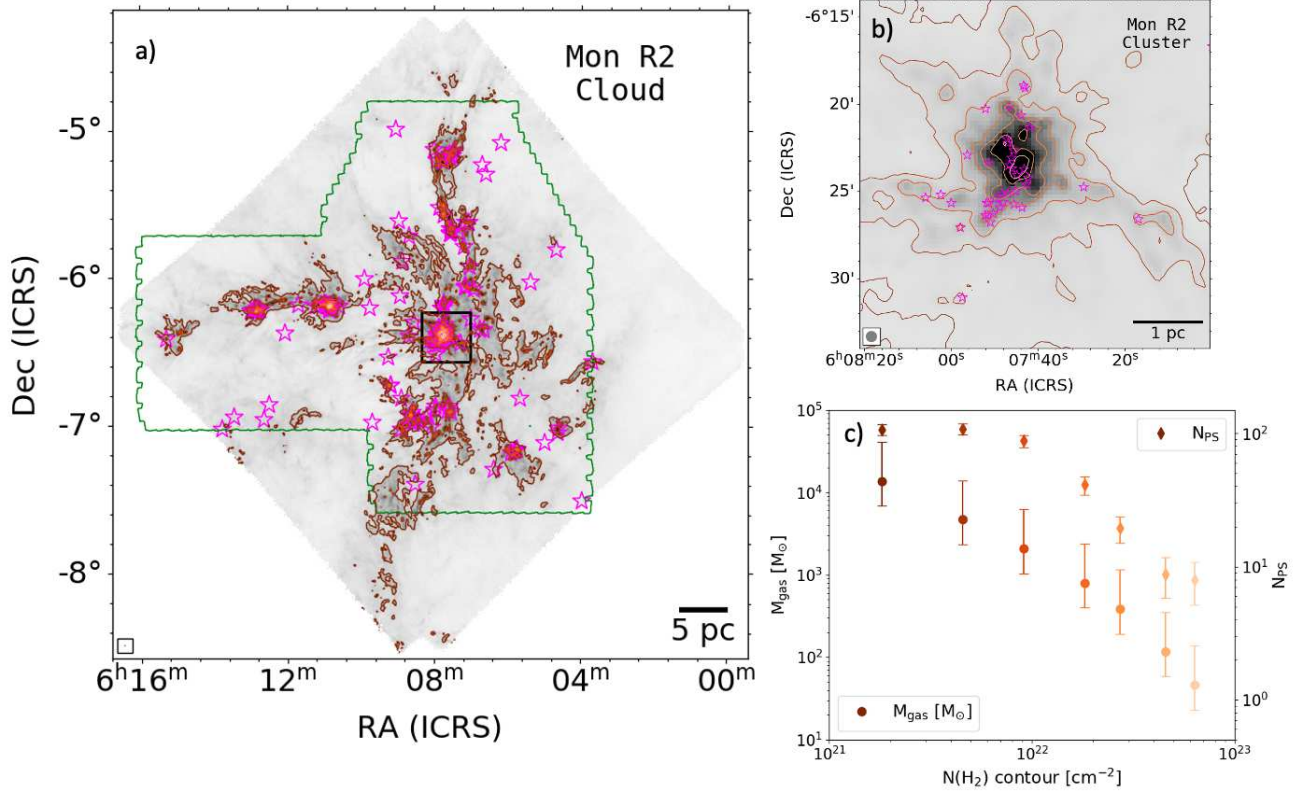


**Figure 1. a):** Gas column density map of the Mon R2 GMC derived from *Herschel* observations<sup>37</sup>. Green contours show the *Spitzer* coverage map that is used for identifying protostars. The brown contours indicate molecular hydrogen column densities of  $N(\text{H}_2) = (2, 5, 10, 20, 30, 50, 70) \times 10^{21} \text{ cm}^{-2}$ , from lowest to highest. Protostars are shown as magenta stars. **b):** Zoom-in view of the  $5 \times 5$  parsec region centered at the Mon R2 cluster that is shown as a black box in the left panel. **c):** Gas mass and the number of protostars enclosed by each contour shown in panels (a) and (b). The colours of the points match the colours of the corresponding contours.

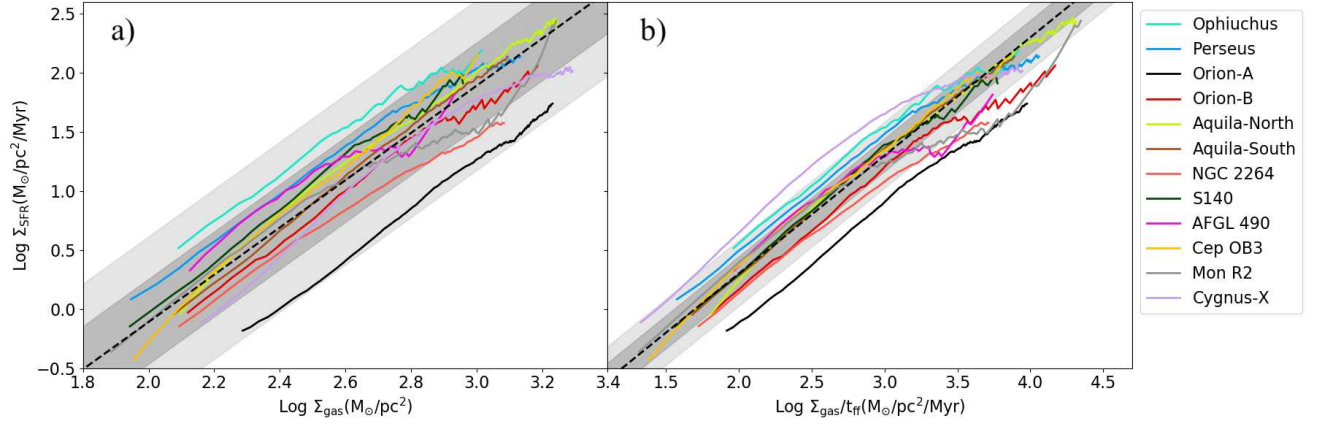


**Figure 2.** a)  $\log \Sigma_{\text{SFR}}$  vs.  $\log \Sigma_{\text{gas}}$  for contours defined on each of the 12 sample clouds (as indicated in the legend) b) Same as (a), but using  $\Sigma_{\text{gas}}/t_{\text{ff}}$  on the horizontal axis. In both panels, black dashed lines show the median best fit relation, using the parameters shown in Table 1; for (b), the black dashed line shows the fit constrained to have a slope of unity, though the best fit for an unconstrained slope is nearly indistinguishable. The darker shaded region shows the interquartile range (IQR) of the data (see Table 1) around the average best fit line. and the lighter shaded region represents two times the IQR.

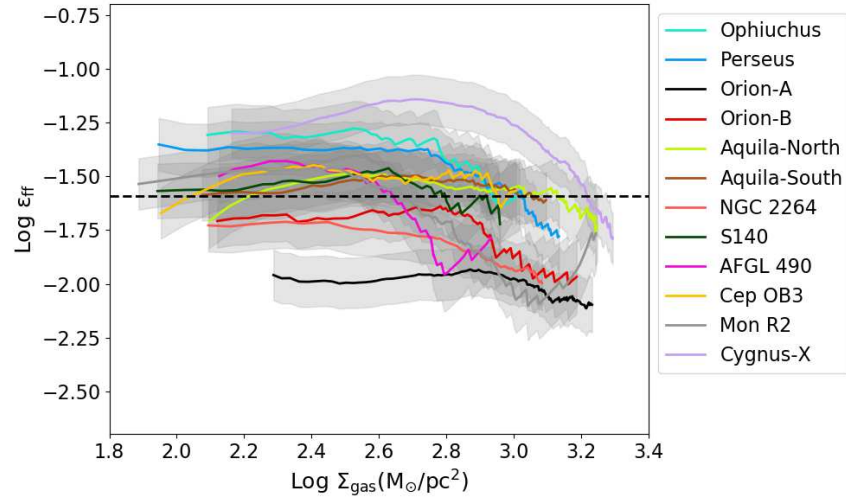


**Figure 3.** Variation of the free-fall efficiency ( $\epsilon_{\text{ff}}$ ) with  $\Sigma_{\text{gas}}$  for our sample of clouds. The uncertainties in  $\epsilon_{\text{ff}}$  are computed by assuming a Poisson distribution on the number of protostars<sup>28</sup>. The median of the logarithm of  $\epsilon_{\text{ff}}$  ( $-1.59$ , see Table 1) is shown by a black dashed line.

## Methods

The input data for our study consist of a matched set of protostellar catalogues and cloud column density maps, such as are illustrated in Figure 1. We use such matched catalogues and maps for the star-forming regions Ophiuchus, Perseus, Orion-A, Orion-B, Aquila-North, Aquila-South, NGC 2264, S140, AFGL 490, Cep OB3, Mon R2, and Cygnus-X.

For protostars, we use the *Spitzer* Extended Solar Neighborhood Archive (SESNA) catalogue compiled by R. Gutermuth et al. (in preparation). The catalogue is constructed using combined *Spitzer* IRAC<sup>38</sup> 3.6, 4.5, 5.8, 8.0  $\mu\text{m}$ , MIPS<sup>39</sup> 24 $\mu\text{m}$ , and near-IR (1.24, 1.67, 2.16  $\mu\text{m}$ ) photometry from the Two Micron All-Sky Survey (2MASS)<sup>40</sup> spanning  $\sim 90^\circ$ , with UK Infrared Deep Sky Survey Galactic Plane Survey (UKIDSS GPS)<sup>41</sup> data added exclusively for our most distant target, Cygnus-X. Sources with excess IR emission are distinguished from field stars and further subdivided into various YSO and contaminant classifications (e.g. background galaxies and unresolved molecular hydrogen shock emission) using a series of reddening-safe colour and flux selections<sup>42</sup>. With a few exceptions<sup>5,22</sup>, prior work on the intracloud KS relation employed protostar identifications that required 24  $\mu\text{m}$  flux measurements (e.g.<sup>19,30</sup>). This requirement strongly limits protostar sensitivity due to confusion from resolved nebulosity and nearby bright sources as are found in young stellar clusters<sup>33,35,43</sup>. SESNA and related *Spitzer* censuses of YSOs make robust protostar identifications that don't require 24  $\mu\text{m}$  photometry, improving protostar completeness under these circumstances<sup>42,44</sup>. In addition, SESNA has a well-measured rate of contamination from extragalactic interlopers and edge-on disks<sup>42,45</sup>, and we can therefore correct statistically for these contaminating effects. The correction procedure is explained in detail in ref.<sup>5</sup>; all our analysis in this work makes use of the statistically-corrected data.

The cloud column density maps we use are described in ref.<sup>5</sup>. Summarising the relevant points here: we construct the maps using *Herschel*/SPIRE and *Herschel*/PACS imaging at 160  $\mu\text{m}$ , 250  $\mu\text{m}$ , 350  $\mu\text{m}$ , and 500  $\mu\text{m}$ , convolved to a common resolution. In each pixel, we fit the observed spectrum using a model for dust emission in which the free parameters are the gas column density and the temperature; in these fits the dust opacity per unit mass at 500  $\mu\text{m}$  is fixed to  $\kappa_{500\mu\text{m}} = 2.90 \text{ cm}^2 \text{ g}^{-1}$  based on the OH4 dust model of ref.<sup>46</sup>. Our column density maps are the results of these fits, and can be expressed equivalently in column of  $\text{H}_2$  molecules,  $N(\text{H}_2)$  or gas mass column  $\Sigma_{\text{gas}}$ ; the two are related by

$$\Sigma_{\text{gas}} = \frac{2m_{\text{H}}}{X} N(\text{H}_2), \quad (2)$$

where  $m_{\text{H}} = 1.67 \times 10^{-24} \text{ g}$  is the mass of a hydrogen atom and  $X = 0.71$  is the hydrogen mass fraction of the local interstellar medium<sup>47</sup>. We also mask pixels where the estimated dust temperature exceeds a threshold value, since in this regime the column density estimate becomes very uncertain – see ref.<sup>5</sup> for details. In the highest density regions the dust emission can be optically thick even at 500  $\mu\text{m}$  and our estimation of column densities may represent the lower limits. However, we are not probing gas beyond  $N(\text{H}_2) \sim 10^{23} \text{ cm}^{-2}$  so the effect on our results is minimal. To the extent that optical depth effects are significant, they would cause us to slightly overestimate  $\epsilon_{\text{ff}}$  at the highest column densities.

Given the input catalogues, we construct the contours within which we measure gas mass, protostar number, and area; our approach is similar to that first explored by ref.<sup>30</sup>. We place the lowest contour at the lowest value of  $N(\text{H}_2)$  such that the resulting contour is entirely enclosed by the footprints of the SESNA catalogue and the column density map. We then place additional contours with uniform spacing of 0.5 magnitudes in V band, where for our OH4 dust model 0.5 mag of extinction in V corresponds to a gas column  $N(\text{H}_2) \sim 5 \times 10^{20} \text{ cm}^{-2}$ , until the smallest contour does not enclose any protostar. The estimates for the minimum and the maximum  $A_{\text{V}}$  are given in Table 1. The result of this procedure is a set of  $(M_{\text{gas}}, N_{\text{PS}}, A)$  triples for each cloud, which forms the basis for our analysis in this work.

We find typical uncertainties of  $\sim 30\%$  in the *Herschel* derived column density maps<sup>37</sup>. We use the same uncertainty factor to estimate uncertainties in derived  $\Sigma_{\text{gas}}$ . Given the uncertainties in assumed emissivity and gas-to-dust ratio, we find the derived masses to be uncertain up to a factor of two. For the uncertainty in the number of protostars enclosed by each  $N(\text{H}_2)$  contour, we use Poisson statistics and further propagate it to obtain the uncertainty in  $\Sigma_{\text{SFR}}$ . The error bars in  $\epsilon_{\text{ff}}$  in Figure 3 correspond to the  $\sqrt{N_{\text{PS}}}$  Poissonian errors, similar to ref.<sup>28</sup>.

## Supplementary Information

Here we compare our results derived from *Herschel* column density maps and the SESNA YSO catalogue to results based on earlier extinction maps and YSO catalogues. For the purpose of this comparison, we focus on the Perseus cloud, and use the extinction maps together with the c2d protostellar catalog (both from ref.<sup>24</sup>). We analyse these data as described in Methods, and plot the resulting correlation between  $\Sigma_{\text{SFR}}$ ,  $\Sigma_{\text{gas}}$ , and  $\Sigma_{\text{gas}}/t_{\text{ff}}$  in Figure 4; the Figure shows our results derived from *Herschel* plus SESNA for comparison. Examining the results, the most obvious difference is that the older data cover a much smaller dynamic range –  $\lesssim 0.5$  decades in  $\Sigma_{\text{gas}}$ , and  $\lesssim 1.5$  decades in  $\Sigma_{\text{gas}}/t_{\text{ff}}$ , compared to  $\gtrsim 1$  decade in  $\Sigma_{\text{gas}}$  and  $\gtrsim 2$  decades in  $\Sigma_{\text{gas}}/t_{\text{ff}}$  for our data. The difference is primarily a result of the extinction maps saturating at high column density, which prevents them from reaching the values of  $\Sigma_{\text{gas}}$  that we can probe using far infrared emission<sup>37</sup>. A secondary contributor is that the SESNA YSO catalogue is more complete in high-density regions. As a result of this difference the linear KS relation between  $\Sigma_{\text{SFR}}$  and  $\Sigma_{\text{gas}}/t_{\text{ff}}$  is significantly more apparent in our data.

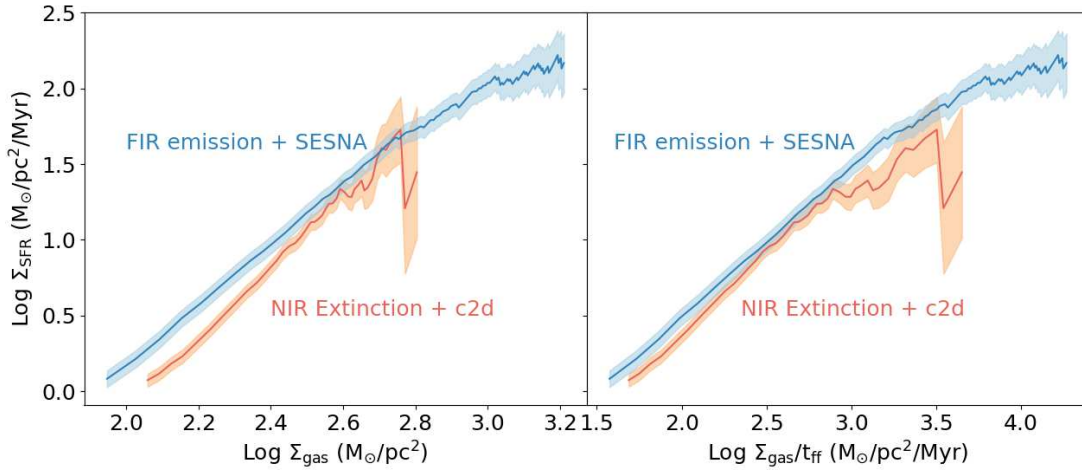


**Figure 4.** Comparison of star–gas surface density correlation plots between our data (far-IR *Herschel*  $N(\text{H}_2)$  gas and SESNA protostars; shown in blue) and a mid-IR extinction map and together with protostars from the c2d catalog (shown in red) for the Perseus molecular cloud.

## Acknowledgements

We gratefully acknowledge funding support for this work from NASA ADAP awards NNX11AD14G (R.A.G.), NNX13AF08G (R.A.G.), NNX15AF05G (R.A.G., R.P.), 80NSSC18K1564 (R.P., S.T.M.), and NNX17AF24G (R.A.G., R.P.), and from the Australian Research Council awards FT180100375 (M.R.K.), DP190101258 (M.R.K.), DP170100603 (C.F.), FT180100495 (C.F.), and CE170100013 (M.R.K., C.F.). S.S.R.O. acknowledges NSF CAREER grant 1748571. This work is based in part on observations made with the *Spitzer* Space Telescope, which was operated by the Jet Propulsion Laboratory, California Institute of Technology under a contract with NASA. Support for this work was provided by NASA through an award issued by JPL/Caltech. This work is also uses observations made with *Herschel*, a European Space Agency cornerstone mission with science instruments provided by European-led Principal Investigator consortia and with significant participation by NASA.

## Author contributions statement

R.P. led the development of the manuscript. R.P. and R.A.G. participated in the data acquisition, data reduction and analysis. M.R.K. suggested the  $\epsilon_{\text{ff}}$  analysis and wrote parts of the manuscript. C.F. and S.K. initiated discussions for comparison of this work with simulations. M.H., S.T.M., P.C.M., S.S.R.O., J.L.P., W.J.F., T.H. and J.L.H. provided useful comments and suggestions that greatly improved the manuscript.

# Figures

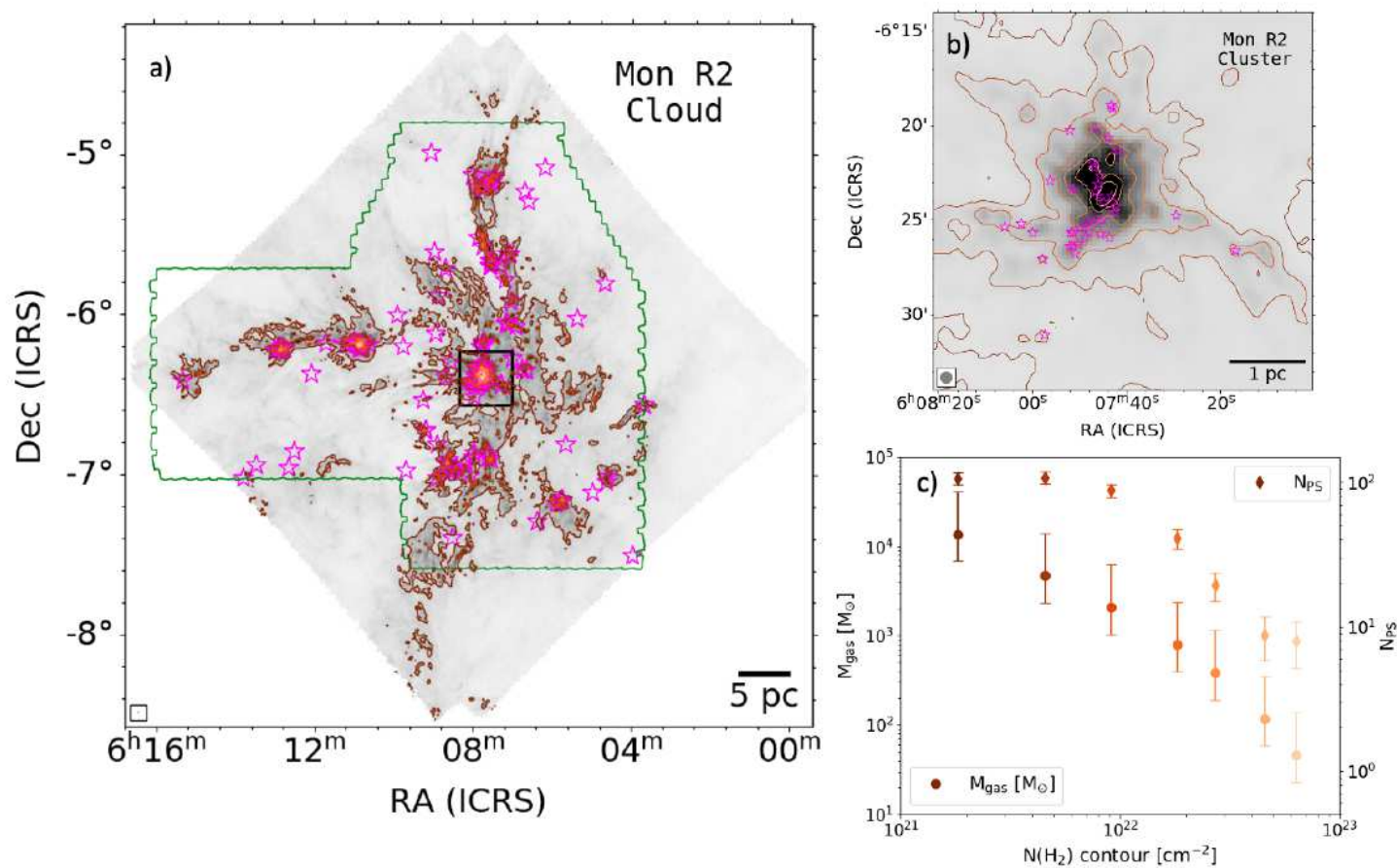
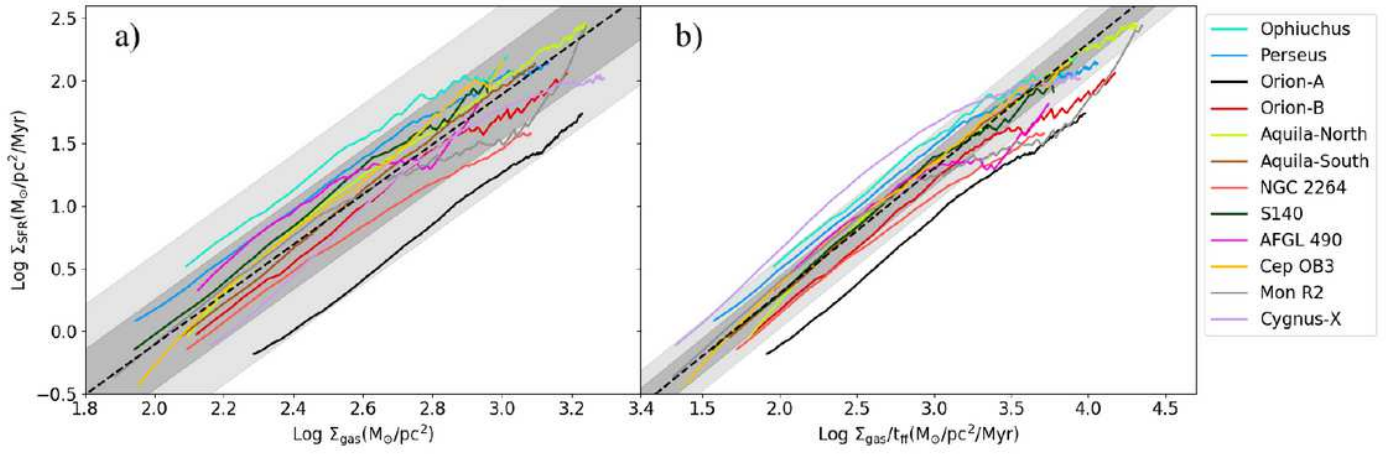


Figure 1

a): Gas column density map of the Mon R2 GMC derived from  $\text{CO}$  observations<sup>37</sup>. Green contours show the  $\text{CO}$  coverage map that is used for identifying protostars. The brown contours indicate molecular hydrogen column densities of  $N(\text{H}_2) = (2, 5, 10, 20, 30, 50, 70) \times 10^{21} \text{ cm}^{-2}$ , from lowest to highest. Protostars are shown as magenta stars. b): Zoom-in view of the  $5 \times 5$  parsec region centered at the Mon R2 cluster that is shown as a black box in the left panel. c): Gas mass and the number of protostars enclosed by each contour shown in panels (a) and (b). The colours of the points match the colours of the corresponding contours.





**Figure 2**

a)  $\log \Sigma_{\text{SFR}}$  vs.  $\log \Sigma_{\text{gas}}$  for contours defined on each of the 12 sample clouds (as indicated in the legend) b) Same as (a), but using  $\Sigma_{\text{gas}}/t_{\text{ff}}$  on the horizontal axis. In both panels, black dashed lines show the median best fit relation, using the parameters shown in Table 1; for (b), the black dashed line shows the fit constrained to have a slope of unity, though the best fit for an unconstrained slope is nearly indistinguishable. The darker shaded region shows the interquartile range (IQR) of the data (see Table 1) around the average best fit line. and the lighter shaded region represents two times the IQR.

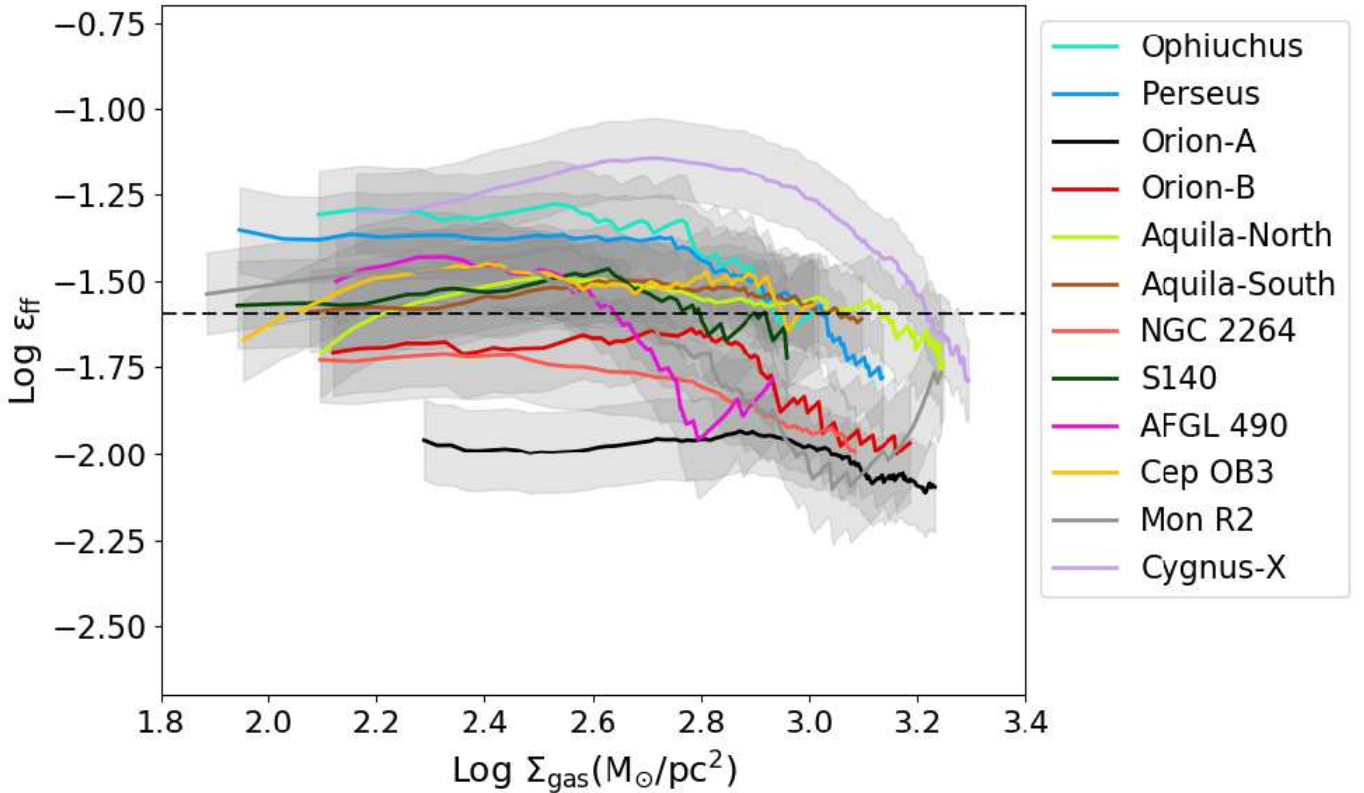


**Figure 3**

Variation of the free-fall efficiency ( $\epsilon_{\text{ff}}$ ) with  $\Sigma_{\text{gas}}$  for our sample of clouds. The uncertainties in  $\epsilon_{\text{ff}}$  are computed by assuming a Poisson distribution on the number of protostars<sup>28</sup>. The median of the logarithm of  $\epsilon_{\text{ff}}$  ( $-1.59$ , see Table 1) is shown by a black dashed line.

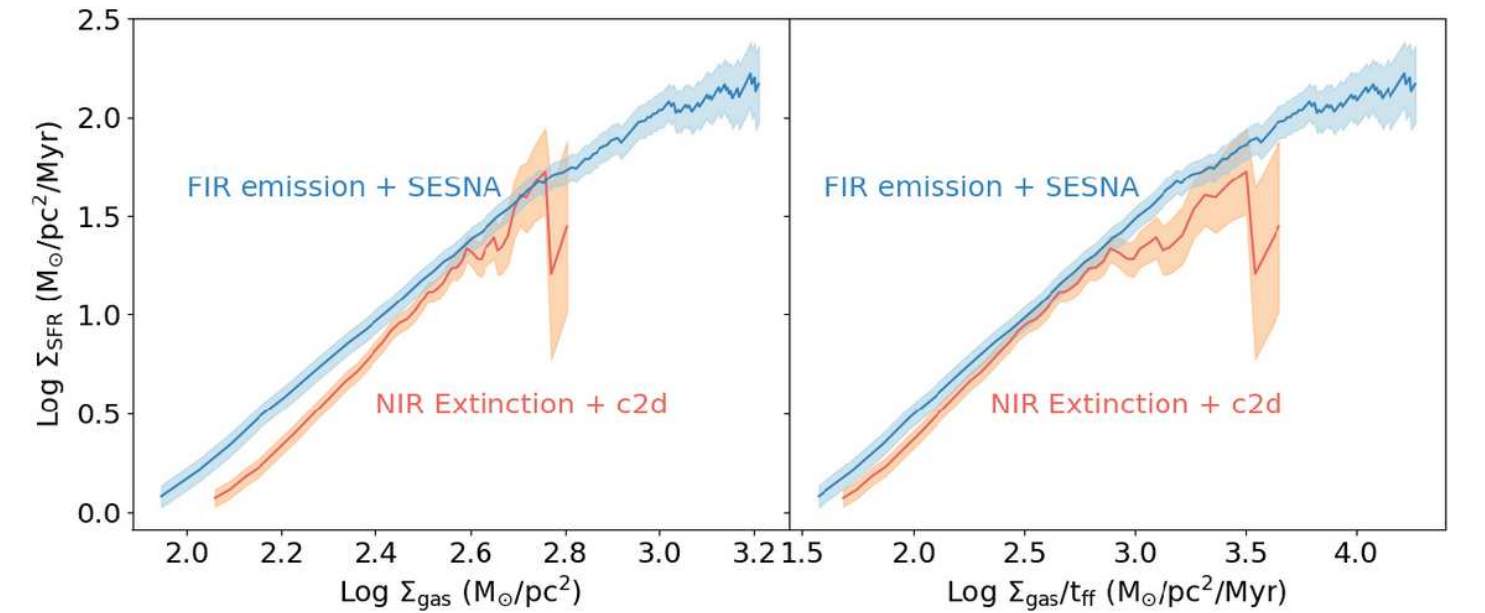


**Figure 4**

Comparison of star–gas surface density correlation plots between our data (far-IR  $\text{H}_2$  gas and SESNA protostars; shown in blue) and a mid-IR extinction map and together with protostars from the c2d catalog (shown in red) for the Perseus molecular cloud.